Construction Materials
Volume 165 Issue CM3

Dimension stone design – kerf anchorage in limestone and marble
Camposinhos and Camposinhos

ice | proceedings

Proceedings of the Institution of Civil Engineers
Construction Materials 165 June 2012 Issue CM3
Pages 161–175 http://dx.doi.org/10.1680/coma.8.00052
Paper 800052
Received 04/11/2008 Accepted 08/03/2009
Keywords: anchors & anchorages/design methods & aids/rock mechanics

ICE Publishing: All rights reserved

ice Institution of Civil Engineers
publishing

Dimension stone design – kerf anchorage in limestone and marble

1 **Rui S. Camposinhos** PhD
Coordinator Professor at ISEP, Polytechnic of Porto, School of Engineering, Porto, Portugal

2 **Rui Pedro A. Camposinhos** MSc
Project Engineer, Stucky Atlântico SA, Porto, Portugal

Rui de Sousa Camposinhos

Digitally signed by Rui de Sousa Camposinhos
DN: c=PT, st=Porto, l=Porto, o=Instituto Superior de Engenharia do Porto, ou=501540709, ou=rdc@isep.ipp.pt, cn=Rui de Sousa Camposinhos, email=rdc@isep.ipp.pt
Date: 2012.07.11 18:39:19 +01'00'

This paper describes a study on kerf anchorage behaviour in three types of stones. Two limestone and various marble specimens were submitted to a series of tests – namely standard absorption, bulk specific gravity and flexural strength tests – to determine their physical and mechanical properties. The paper focuses on the results of tests carried out according to the ASTM *Standard Test Method for Strength of Individual Stone Anchorages in Dimension Stone*. These tests were performed on a stiff rail continuous anchorage system on both the front and rear kerf legs. Stress analysis and finite element method calculations were the basis for the proposed semi-empirical formula to estimate this anchorage system's breaking load under the above-mentioned conditions. Through a general but practical example, it is shown that a design focused on the bending strength of stone panels, to the detriment of the kerf anchorage, is an unsafe and yet common practice. The paper emphasises that designing stone cladding systems with continuous kerf must take into account different effects in order to evaluate the effective stress in the critical region of the kerf geometry. Separate stress concentration factors are proposed to account for the kerf geometry and the specimens' specific properties.

1. Introduction

Stone wall systems have been employed to achieve a wide range of architectural styles, aesthetic effects and appearances. Generally, thin stone wall systems are used in all environments and can have various finishes.

Granites have had a long history of durable service, and certain marbles have a long history of successful use. However, some marble types, particularly some white marbles of pure calcite, have been found not to be durable materials because of their susceptibility to deterioration from heating and cooling cycles. Travertine, limestone and sandstone have a good history when applied as thick stone wall elements, but their service history as thin stone wall elements is fairly limited, particularly their durability. Inadequate initial evaluation of material durability and panel strength resulted in varying degrees of distress in some claddings. Although early stone cladding was installed with little thought to structural analysis, current evaluation techniques should predict capability by checking characteristics that were probably ignored by the initial engineering. Nevertheless, most failures in stone wall systems can be attributed to the fastening system (Lewis, 2007). Panel cracking, displacement or other failures can occur at locations where anchors are inadequately or improperly connected to the stone. Poor construction is often the result of poor quality and tolerance control during panel fabrication and/or erection. Moreover, damage during handling operations can also result in panel cracking, some of which may not become evident for several years. Yet, it must be recognised that a lack of information on stone cladding dimensioning and design rules is one of the most common reasons, if not the main reason, for the majority of failures (Lammert and Hoigard, 2007; Lewis, 1995).

This paper focuses on the study of kerf anchorage behaviour regarding three types of stones. Two limestone and various marble specimens were submitted to a series of tests – namely standard absorption, bulk specific gravity and flexural strength tests – to determine their physical and mechanical properties. The paper focuses mainly on the results of a series of tests carried out

according to the *ASTM Standard Test Method for Strength of Individual Stone Anchorages in Dimension Stone* (ASTM, 2004). These tests were carried out in a stiff rail continuous anchorage system on both the front and rear kerf legs.

Stress analysis and finite element method (FEM) calculations were the basis for the proposed semi-empirical formula to estimate this anchorage system's breaking load under the above-mentioned conditions. Separate stress concentration factors are proposed to account for the kerf geometry and the specific properties of the stone specimens.

2. Design principles

Stone wall systems are traditionally constructed as a curtain wall or veneer, in which no building loads are transferred to the stone panels. Typically, the stone wall system must bear all lateral loads, such as those caused by wind and earthquakes, as well as vertical loads resulting from its own weight. The thermal-related expansion and shrinkage of the stone units may generate localised pressure where they come in contact with one another. Although loads such as accidental impacts, construction handling and transportation must also be taken into account in the design, these factors are not covered by the present paper. Design is not restricted to dimension stone elements, since the fixing elements must also be designed accordingly.

Although the wind load is normally used to determine the load case, earthquake loads must not be neglected in relevant seismic areas.

The mechanical behaviour of structures, particularly stress-deformation behaviour, is greatly influenced by the respective materials. Based on that behaviour, most engineering materials can be categorised as brittle, ductile or quasi-brittle (Shah *et al.*, 1995). The stress quickly drops to zero when a brittle material fractures, whereas large deformation at constant stress occurs when a ductile material yields. On the other hand, a quasi-brittle material is characterised by a gradual decrease in post-peak stress.

Procedures to estimate stone slab dimensions based simply on permitted bending stress calculations are, in most cases, not adequate to ensure safety.

It must be emphasised that, for some cladding systems, there is relevant information about design methods or approaches (Camposinhos and Camposinhos, 2009; Lammert and Hoigard, 2007; Moreiras *et al.*, 2007; West, 2004), which exceed the traditional 'bending at midspan' stress calculations, often referred to as allowable stress design.

3. Kerf anchorage

A kerf is a sawcut groove or slot in the edge of a stone panel. A kerf clip or kerf bar is a flat bar or thin plate configured to engage a sawcut slot in the stone edge. These profiles are fastened to a support frame or connected directly to the building structure by bolts or anchors, thus providing the essential mechanical connection between the stone and the structure.

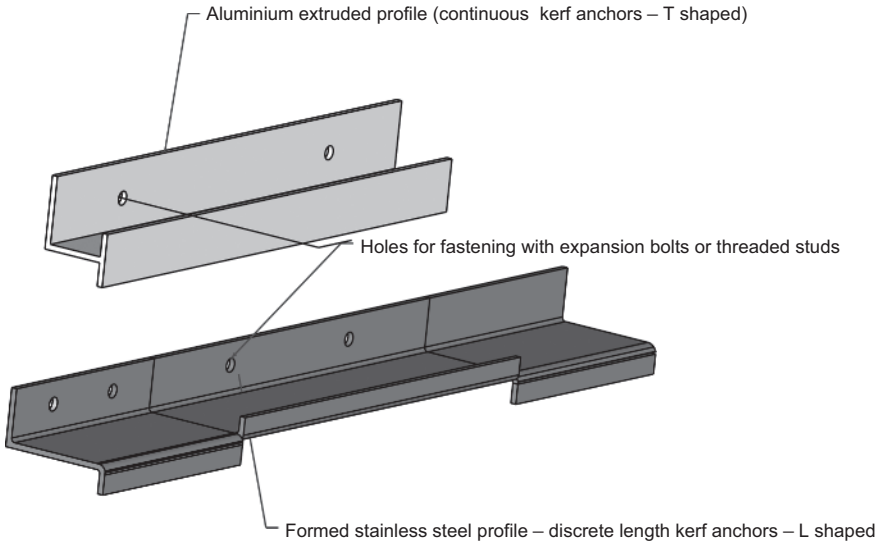

Figure 1. Kerf anchor profiles in discrete and continuous length configurations

Figure 1 illustrates typical kerf anchor configurations, normally in formed stainless steel or extruded aluminium profiles. Other metals may be used if properly protected against moisture and galvanic action. They may be continuous or discontinuous and are typically located in the top and bottom edges for easier access and alignment during installation.

The structural capacity of this type of anchorage depends essentially on the combined shear and flexural strength of the stone's fin or leg.

The main issues regarding assembling stone panels using kerf anchors revolve around considerations which are implicit in the design; they are numbered and illustrated in Figure 2.

(*a*) Placing a plastic or metal adjustment bearing shim slightly larger than the anchor's fastened face [1].
(*b*) Preventing the connection from slipping after vertical adjustment with a diagonally slotted washer plate, welded washer or serrated anchor and washer [2].
(*c*) Attaching the anchor with a fastener to a back-up structure [3].
(*d*) Avoiding a kerf anchor (brake-formed split-ear shape down) or extruded shape that fits into a sawn kerf [4] misalignment to prevent prying on kerf due to inaccurate fabrication or installation.
(*e*) Maintaining clearance to avoid contact and weight transfer (unless designed to stack) [5], thus allowing for movement, creep, expansion, and fabrication and installation tolerances.
(*f*) Placing a plastic or stiff rubber bearing shim to level, separate or to prevent bearing of stone kerf fin on anchor radius [6].
(*g*) Maintaining clearance to avoid point loading [7, 10] at the kerf at the top and bottom of stone.
(*h*) Placing backer rod or foam tape at proper depth [8] to prevent a three-sided sealant bond.
(*i*) Sizing joints [9] to allow for hardware, tolerances, clearances, appropriate movement and joint filler capability; ensuring clearance and thus avoid point loading at the top and bottom. Kerf filling must be continuous with sealant to top of kerf to prevent moisture accumulation.
(*j*) Minimising distance [12] to reduce eccentric weight on the anchor (ASTM, 2003; Camposinhos and Amaral, 2007).

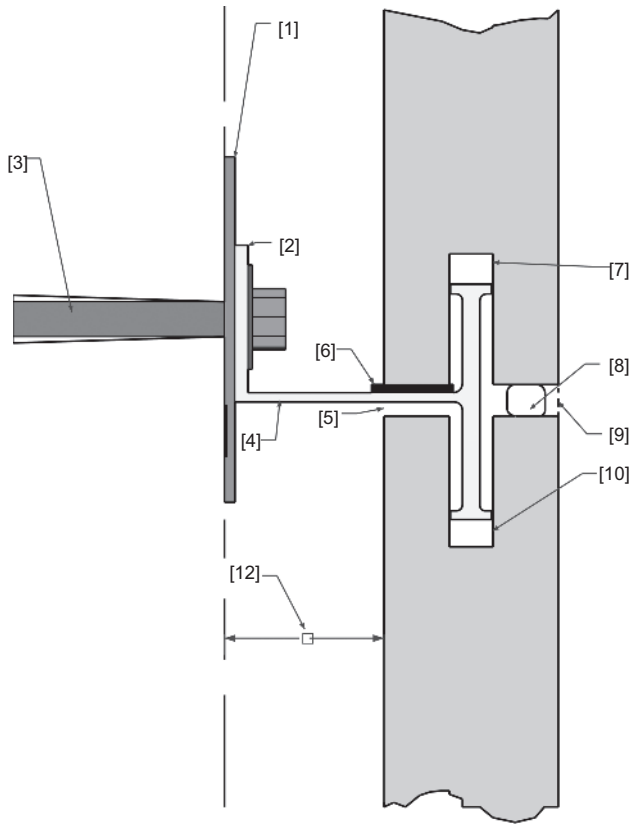

Figure 2. Typical cross-section of kerfed stone cladding systems

The core parameters affecting the anchorage capacity have been depicted (Lewis, 1995), namely and mainly in the following manner (Figure 3).

(*a*) Kerf slot width (t_k) the distance across the saw cut varies due to the original saw blade thickness and the blade's reliability of plane and rotation. The degree of wear resulting in a thinner blade which tends to veer.
(*b*) The thickness of the stone fin (t_f) remaining on the panel edge, after kerf anchorage assembly determines its potential strength. The distance from the inside face of the kerf to the finished face varies according to the stone panel gauge after having been sawn and the stone panel thickness, in accordance with the previously mentioned factors.
(*c*) The depth of contact (D), namely, the depth to which the kerf clip's leg contacts the stone within the stone kerf.
(*d*) The length to which the kerf clip's leg is engaged, taking into account that the actual length is not necessarily the effective length of engagement.

Note that the continuous kerf rail in the stone edge does not provide a continuous support for the stone unless the kerf rail is much stiffer than the stone panel.

In fact, when the support rail's stiffness (which depends on the rail itself, on its cross-section's moment of inertia and modulus of elasticity) is less than the dimension stone's stiffness (determined by the stone's thickness and modulus of elasticity) along the span of the dimension stone, the entire kerf rail length will not act as a continuous support (Conroy and Hoigard, 2007; Lewis, 1995; West and Heinlin, 2000).

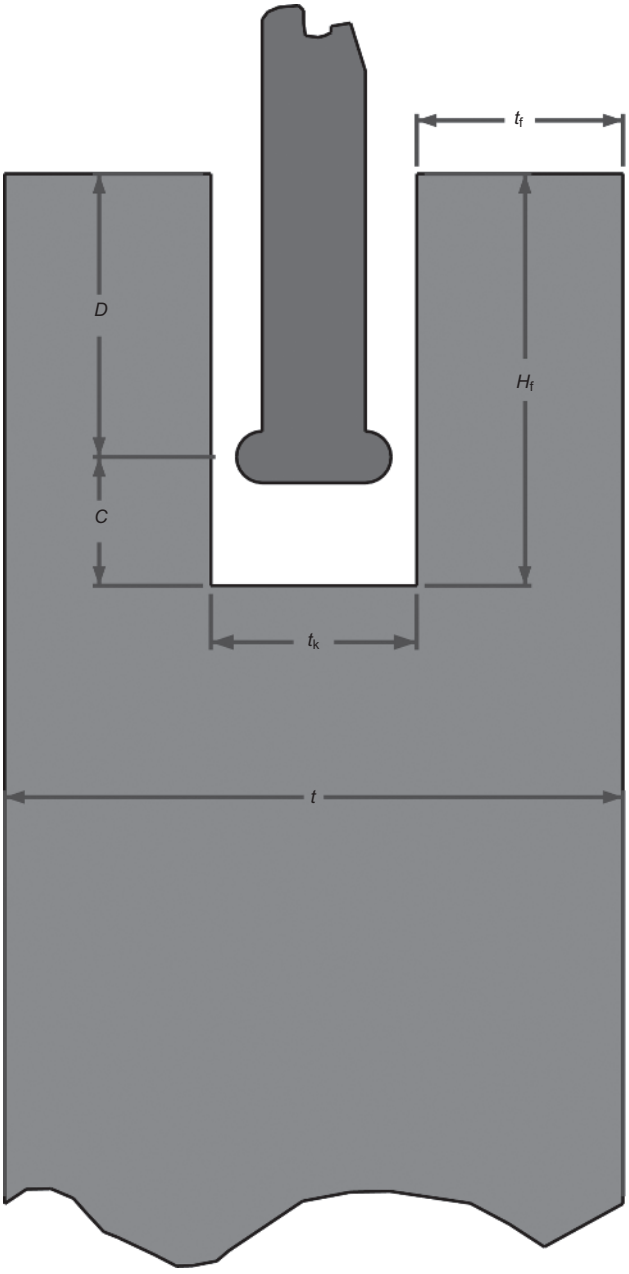

Figure 3. Kerf slot width, fin and depth of rail contact

4. Case study

In the present study kerf anchorage behaviour based on a number of mechanical tests was analysed using two sedimentary and one metamorphic Portuguese stones.

This study aimed to investigate the relationship between flexural strength and breaking load at the kerf anchorage. Stiff rails were used to ensure a continuous support.

The tests were helpful in gaining a better understanding of the rupture behaviour of a common kerf anchorage. The test results were the basis for calibrating a simple formula that can be used to estimate the breaking load of the stone at the kerf anchorage.

4.1 Stone type and specimens

4.1.1 Lithological description

Two limestone and one marble specimens were studied (Figure 4).

(*a*) Molianos, an oolitic limestone formed of shells and shell fragments, is practically non-crystalline in character and found in massive deposits. This limestone is characteristically freestone, without cleavage planes and has a remarkably uniform composition, texture and structure. It has a high internal elasticity and adaptability to extreme temperature changes. Molianos is known by various commercial names, such as Gasgogne Beige or Gasgogne Blue, Guido Limestone or Porto Velho.

(*b*) Lioz**,** a beige semi-crystalline limestone with coarse elements, bioclastic and calciclastic. It is a biosparite

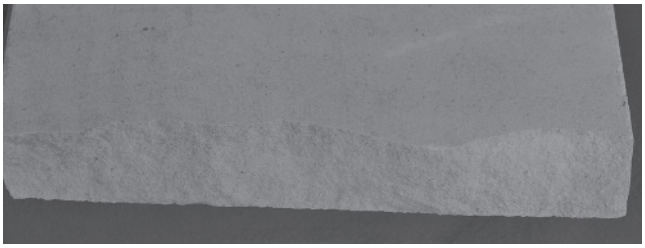

(a)

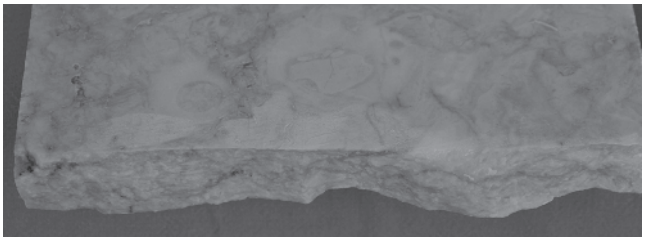

(b)

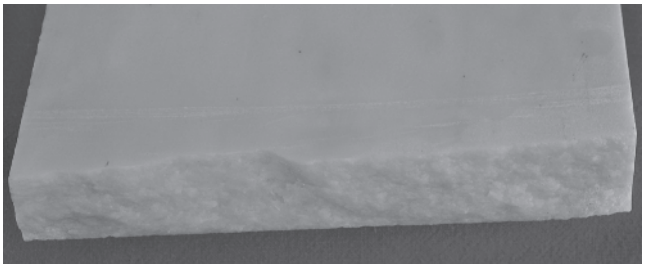

(c)

Figure 4. Images of three of the specimens studied, all samples are 30 mm thick

Sample	Type	Water absorption (EN 13755)	Volumic mass: kg/m^3	Open porosity (EN 1936)
Molianos	Limestone	3·1%	2456	6·2%
Lioz	Limestone	0·1%	2658	0·4%
Estremoz	Marble	0·07%	2770	0·2%

Table 1. Water absorption, volumic mass and open porosity of the stones studied

– microsparite that has been slightly affected by metamorphism. This limestone is often used as dimension stone and is usually well consolidated and has minimum graining or bedding direction.

(*c*) Estremoz, a high quality, fine- to medium-grained marble. This cream-white stone has excellent mechanical-physical properties and is aesthetically pleasing. These marbles have been quarried since the Roman period and throughout the Middle Ages.

4.1.2 Physical and mechanical properties

Samples were tested both wet and dry. The wet samples were soaked in water at 22℃ for a minimum of 48 h and a maximum of 120 h. The dry samples were dried prior to testing in a humidity-controlled oven at 65℃ and gradually cooled to 22℃. The relevant mean values of the physical characteristics of the samples are shown in Table 1.

The stones were tested in accordance with EN 1926 (CEN, 2006) to determine their unconfined compressive strength (UCS). Forty-five cylindrical samples were tested in dried conditions. The test results are shown in Table 2.

Flexural strength was determined with three-point load tests. These tests were carried out on 33 prism samples (50 mm × 30 mm cross-section) and on 59 slab samples with a (200 mm × 30 mm) cross-section in accordance with European Standard EN 12372 (CEN, 1999). Hence, all specimens had a total length of 180 mm and were placed on rollers with a 150 mm gap. The samples were tested in dried conditions with a gang-sawn finish on the lower surface. The bending strength per type of stone and the number of tests are shown in Table 3.

Sample	UCS (average): MPa	Quantity
Molianos	92·81	15
Lioz	88·90	15
Estremoz	85·91	15

Table 2. Average unconfined compressive strength of stones studied as per EN 1926

The last two columns in Table 3 indicate the average flexural strength value and, as the tested specimens had the same span-to-thickness ratio, these values were adopted in the study.

4.2 Anchorage strength tests

Specific tests were performed on the slab specimens to evaluate the strength of the kerfed edges.

All anchorage strength tests were performed according to the ASTM C 1354 test method (ASTM, 2004) using specimens with nominal dimensions of 400 mm × 200 mm by 30 mm thick and with both faces sawn. All specimens were tested after being in dry storage for over 1 week, without any additional wetting or drying procedures.

The test configuration is shown in Figure 5.

The kerf anchor was installed in only one of the edges of the stone specimen and the opposite edge was placed over a roller support.

The load was applied at a close distance from the kerf anchorage ($(t+H_f)$; Figure 3) to avoid interference in the failure mode.

The actual load applied to the anchor, which was less than the total applied load, was calculated using simple statics principles.

4.3 Performing the tests

The anchors were bolted to a cold-formed channel support which was attached to a heavy steel reaction frame using threaded rods. The testing machine has a load cell capacity of 10 kN. Load values were displayed on a digital readout with a peak value memory.

The load was applied at a constant rate of approximately 0·02 kN/s. Precautions were taken to ensure parallel alignment between the loading line and the kerf bottom.

The anchor knife and the kerf's leg formed an angle slightly greater than 90° to ensure that the contact line was parallel to the kerf's slot (Figure 6).

	Prisms *FS*: MPa	c.v.	Qty	Slabs *FS*: MPa	c.v.	Qty	*FS* average: (MPa)	c.v.
Molianos	12·64	9·3%	9	9·10	10·1%	29	10·16	19·21%
Lioz	14·63	7·9%	12	12·94	9·5%	30	13·62	10·63%
Estremoz	20·29	11·5%	12	19·8	9·9%	21	19·96	10·42%
Total	–		33	–		59	–	

FS, flexural strength; c.v., coefficient of variation; qty, number of tests.

Table 3. Flexural strength of tested stone according to EN 12372

Tests were performed using continuous steel stiff rail anchors installed in the continuous kerf. The typical kerf slot dimensions were 7 mm wide and 26 mm deep in the stone edge. The anchor rail was fitted inside the kerf groove at a measured depth of 13·5 mm. As the upper and lower kerf legs were slightly different in thickness, each specimen's dimensions were measured after and before every test. Similarly, measurements were made for the slot's contact depth.

Some authors (Conroy and Hoigard, 2007; Lewis, 1995) have reported both laboratory and in-service kerf failures of curtain wall systems with full-width aluminium extrusion kerf hardware. These failures typically occur in the form of multiple short kerf breaks starting at the outer panel edges and proceeding inward towards the panel centre. In order to avoid this type of failure and to ensure that the kerfed stone cladding panels form a plate supported along two edges, the stiff steel rails were used to prevent any deflection between the kerf legs (Figure 6). During testing, the authors found that the cold-formed channel support did not undergo any vertical or lateral displacement. Furthermore, the contact was defined at a precise contact depth consisting of a support line between the kerf leg and the steel rail of the kerf anchorage, as mentioned before.

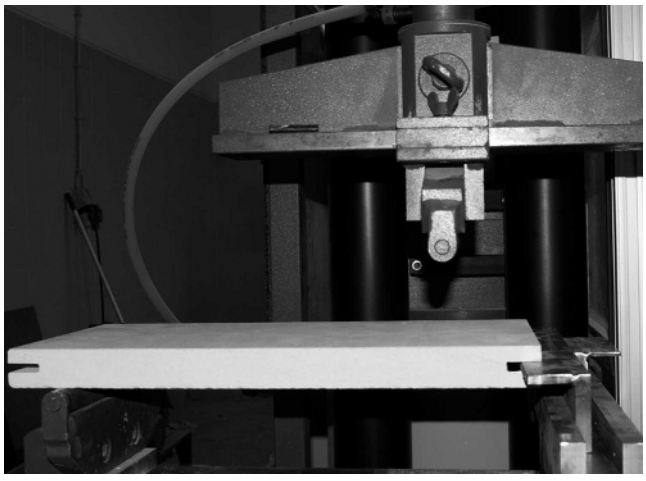

Figure 5. Test arrangement before knife edge adjustment

5. Results

A total of 106 tests were performed to determine the pullout load failure in accordance with Equation 1, which is the formula given in ASTM C1354 (ASTM, 2004).

$$1. \quad P = \frac{F \times A}{L}$$

With reference to Figure 7: A is the distance between the roller support and the acting load (F); and L is the span, namely the distance between roller and kerf supports.

The breaking load test results are summarised in Table 4.

The 106 tests were performed on 27 slab specimens, and generally four tests were performed for each panel, two legs for each slab, except for one Molianos slab for which only one test was performed. All tests resulted in kerf leg failure. The spalling angle for the same type of stone was very similar. The spall failure orientation, angle, α, in Figure 6 was measured for all of the 106 spalls at three separate locations.

The average value obtained as well as the range values of angle α are shown in Table 5, along with the variation coefficient.

The shape and configuration of various spalls are illustrated in Figure 8 for each type of stone. Figure 9 shows a comparison of side-by-side spall angles.

5.1 Analysis

A considerable number of theories have been proposed relating uniaxial to biaxial or triaxial stress systems. For brittle or quasi-brittle materials, the maximum stress criterion, or Rankine criterion, has been applied. In this criterion, it is assumed that failure occurs in a multiaxial state of stress when

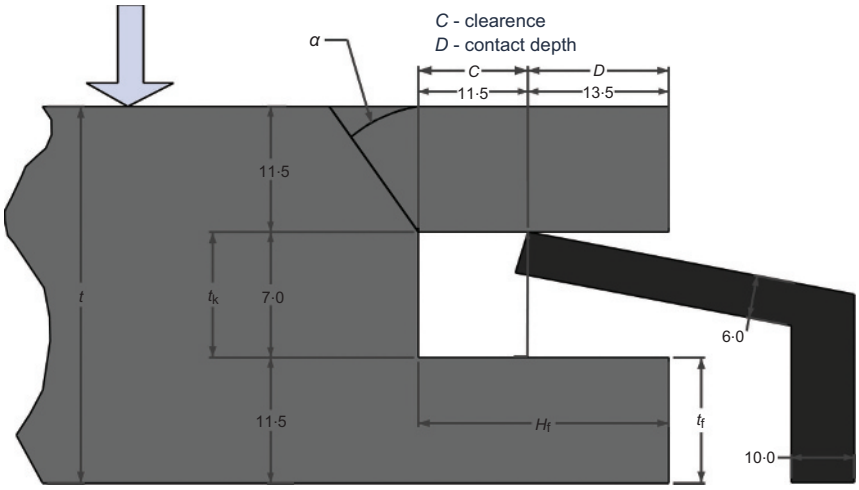

Figure 6. Typical dimensions in mm of anchor cut-off – kerf groove, legs and contact depth for kerf steel angle

either a principal stress reaches the uniaxial tensile strength, σ_{ut} or a principal compressive stress reaches the uniaxial compressive strength, σ_{uc}. As for natural stone, σ_{uc} is considerably greater than σ_{ut}, and in the present case the principal compressive stress is thus neglected.

The nominal principal tensile stress in the critical plane of the kerf's leg (Figure 10) is given by:

$$2. \quad \sigma_{nom} = \frac{\sigma_x + \sigma_y}{2} + \frac{1}{2} \times \sqrt{(\sigma_x - \sigma_y)^2 + 4 \times \tau_{xy}^2}$$

$$3. \quad \sigma_x = \frac{6 \times P \times C}{B \times t_f^2}; \sigma_y = 0$$

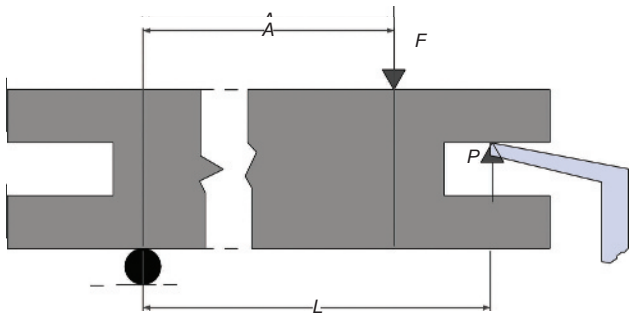

Figure 7. Test arrangement and typical lengths: L = 290 mm; A = 232 mm

$$4. \quad \tau_{xy} = \tau \sim \frac{P}{B \times t_f}$$

Note that the shear stress in this region is assumed to have an average value when compared with the exact formula.

Substituting Equations (4) and (3) in Equation (2), for the maximum principal tensile stress, σ_{nom}, we obtain:

$$5. \quad \sigma_{nom} = 3 \times \frac{P \times C}{B \times t_f^2} + \sqrt{9 \times \left(\frac{P \times C}{B \times t_f^2}\right)^2 + \left(\frac{P}{B \times t_f}\right)^2}$$

When comparing σ_{nom} with the flexural strength, FS, for each type of stone, it is necessary to multiply the value from Equation (5) by an effective concentration factor, K_{eff}.

$$6. \quad \sigma_{nom} \times K_{eff} = FS$$

By substituting Equation (6) in Equation (5), the value of K_{eff} is obtained, which is the effective or global stress concentration factor at the critical failure line.

$$7. \quad K_{eff} = \frac{FS \times B\left[\sqrt{C^2 \times (9C^2 + t_f^2)} - 3C^2\right]}{C \times P_u}$$

where K_{eff} is the effective concentration factor; P_u is the breaking load; FS is the flexural strength; B is the slab width; $C = H_f - D$ is the clearance distance between the contact point

Stone	Type of stone	Number of tests	Average value (P): kN Figure 7	c.v. for P (%)	Average value (F): kN Figure 7
Molianos	Limestone	34	1·65	10·8%	2·04
Lioz	Limestone	36	2·55	19·3%	3·19
Estremoz	Marble	36	2·48	13·4%	3·09
–	Total	106	–	–	–

Table 4. Cell applied load, F, and breaking load, P, at the kerf anchor

of the anchor and the bottom of the kerf; and t_f is the leg width.

These values are plotted in Figure 11 for the tested stone and replace, for each test, the breaking load value, P_u, the medium value of the flexural strength given in Table 3 and the corresponding specimen dimensions in Equation (7).

The average values obtained for K_{eff} were 2·12 for Lioz, 2·40 for Molianos and 3·22 for Estremoz. It must be pointed out that these concentration factors include, not only stress concentration due to the abrupt geometry change near the edges of the stone, but also magnification due to the intrinsic properties of quasi-brittle materials, such as natural stones, caused by particles, grains or inclusions, or simply regions of microscopically irregular surfaces causing topological interference (Sauoma *et al.*, 2003).

5.2 Geometrical stress concentration factors

The presence of shoulders, grooves, holes, and so on also modify stress distributions, which are obtained through elementary stress design formulas and are based on the members having a constant section or a section with a gradual contour change, so that localised high stresses occur and are measured by a stress concentration factor. In this case the elastic 'theoretical' or 'geometric' stress concentration factor, K_t, can be defined as the ratio between the actual maximum stress and the nominal stress:

$$8. \quad K_t = \frac{\sigma_{max}}{\sigma_{nom}}$$

where K_t is the elastic 'theoretical' or 'geometric' stress concentration factor; σ_{max} is the maximum stress to be expected in the member at the critical section; and σ_{nom} is the reference or nominal principal tensile stress at the critical section according to Equation (6).

In some cases, a theoretical factor can be derived for K_t based on the theory of elasticity, or it may be obtained through a laboratory stress analysis experiment. The universal availability of powerful, effective computational capabilities, usually based on the finite element method (FEM), has altered the need for and use of stress concentration factors. Nevertheless, it is desirable to compare the values obtained through both methods. In this case (Figure 12), typical kerf cross-section geometry is illustrated through a macro photograph.

Based on the photo-elastic tests of Leven and Hartman (1951) and of Wilson and White (1973), cited by Pilkey and Pilkey (2007) the corresponding K_t can be determined for the present case. A value of K_t : 1·58 can be obtained using chart 3.9 in the bibliography of Pilkey and Pilkey (2007).

5.3 Finite element approach

A two-dimensional (2D) finite element model representing a kerf anchorage configuration was developed to determine the stone's stress state in the vicinity of the anchor.

The model uses a four-node formulation for membrane elements with an isoparametric formulation for the translational in-plane stiffness component.

A linear elastic analysis was performed using a refined mesh in the anchor's vicinity in order to capture the elastic state of stress at the radius fillet as shown in Figure 12. Three runs

Stone	Type	Spall angle α: degrees	c.v.	Min α: degrees	Max α: degrees
Molianos	Limestone	15·8	12·5%	19·4	13·4
Lioz	Limestone	23·9	23·1%	32·7	16·6
Estremoz	Marble	44·5	10·1%	52·6	39·0

Table 5. Spall angle α measured (Figure 6)

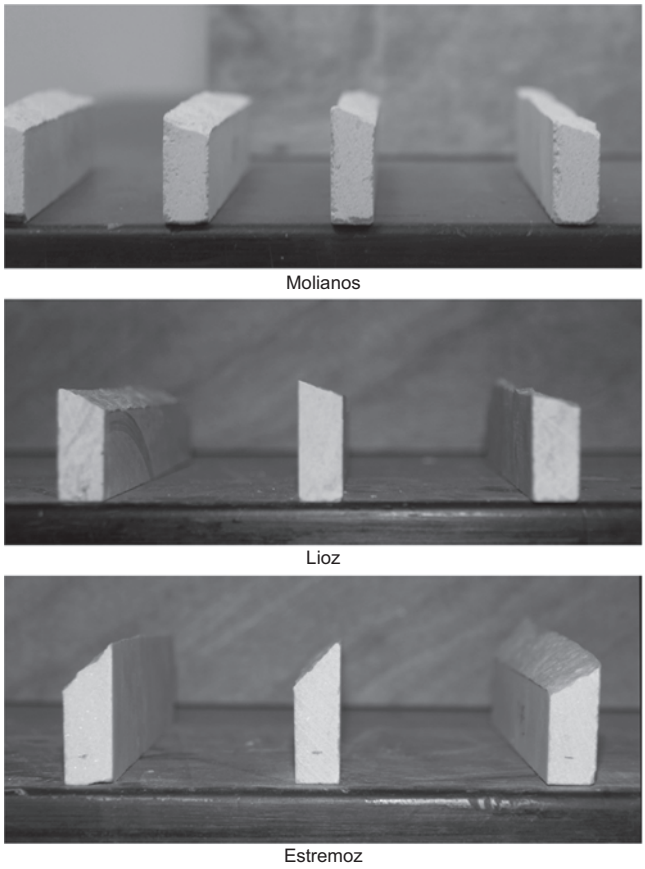

Figure 8. Generated spalls after testing using a continuous stiff rail in Molianos and Lioz limestone and in marble Estremoz specimens

were made taking into account the self weight of the panels and the average breaking load values for each type of stone, according to Table 4 (Figures 6 and 7).

The principal stress values are mapped in Figures 13, 14 and 15 for each stone type by applying the average breaking load value from tests.

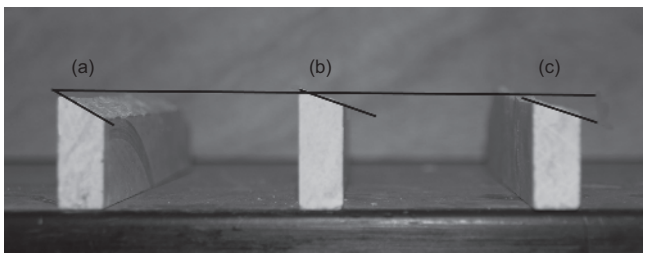

Figure 9. Generated spalls after testing from left to right: (a) Molianos; (b) Lioz and (c) Estremoz specimens

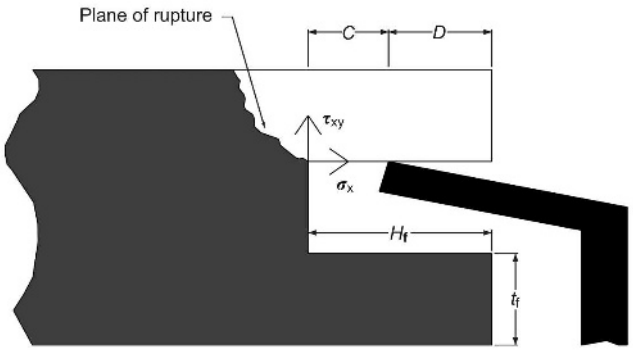

Figure 10. Normal and shear stress at a critical kerf leg section

5.4 Comparison of peak stress values

Table 6 shows the calculated peak-factored elastic stresses, using Equation (8), which are summarised and compared with the maximum principal tensile stress obtained with the FEM.

Note that the authors confirmed that the stress values obtained in tests coincided with the stress obtained in the prism samples using the same FEM formulation as that was used for the kerf-supported specimens.

The values in columns (4) and (6) in Table 6 may be used to compute the corresponding average elastic concentration factor value (Table 7) when the FEM is used (K_t : 1·67). This value is in agreement with the one used in Equation 8 (K_t : 1·58).

5.5 Magnification factors

Standard design methods for engineering structures and components under static loading are usually based on avoiding failure caused by yielding/plastic collapse or buckling. The loading resistance is determined based on conventional solid mechanics theories of stress analysis. Conventional design procedures to prevent fatigue failure are based on experimental results for particular geometric details and materials. None of these procedures are capable of taking into account the effects of severe stress concentrations or crack-like flaws. The presence of such flaws is more or less inevitable to some extent in practical manufacturing and is a characteristic of quasi-brittle materials such as natural stones.

The strength of a material can, in the simplest terms, be viewed as the maximum stress which the material can sustain under given conditions. Theoretical strength calculations often over-estimate the strength if they do not incorporate mechanisms to account for material defects such as cracks. To propagate material defects, the theoretical strength must be overcome only locally, within a 'stress concentration' produced by these flaws; hence the effective strength of the material is lowered.

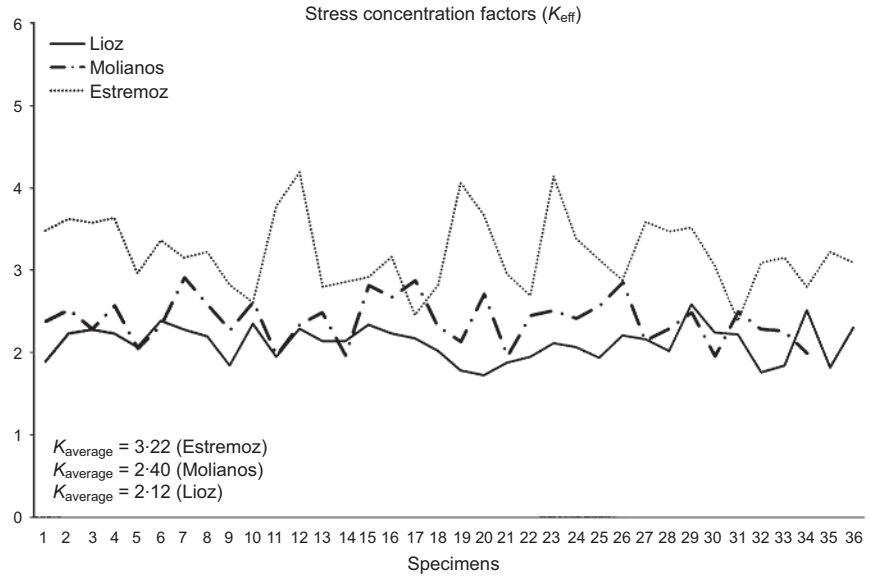

Figure 11. Effective stress concentration factors for kerf anchorages in Molianos, Lioz and Estremoz

Fracture mechanics methods are particularly useful in making fitness for purpose assessments of the effects of flaws. An important effect arises when the crack affects the net cross-section area either in the case of a through-thickness crack in a plate of finite width, or in the case of remaining ligaments between the crack front and a free surface for part-thickness cracks (Albrecht and Yamada, 1977; Sauoma *et al*., 2003; Shah *et al*., 1995).

When a crack is located in a region of geometric stress concentration, there will be a further increase in the stress. The overall effect depends on the relative size of the crack and the stress concentration zone. In this situation, a stress intensity magnification factor (M_c) is required to represent the necessary amplification (Albrecht and Yamada, 1977; Rooke and Cartwright, 1976).

5.6 Effective stress concentration factor

Accordingly, the effective concentration factor, K_{eff}, obtained through Equations (6) and (7), can be broken down to isolate the stress concentration caused by the kerfed edge geometry

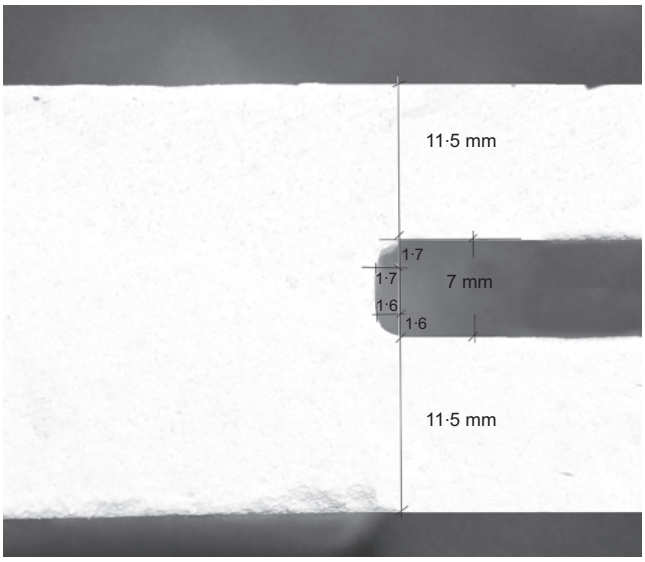

Figure 12. Kerf geometry and dimension in mm of edge cross-section

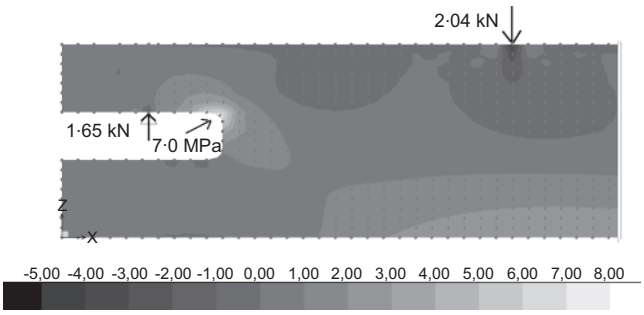

Figure 13. Finite element method calculation of maximum principal stresses at bottom of kerf: Molianos limestone

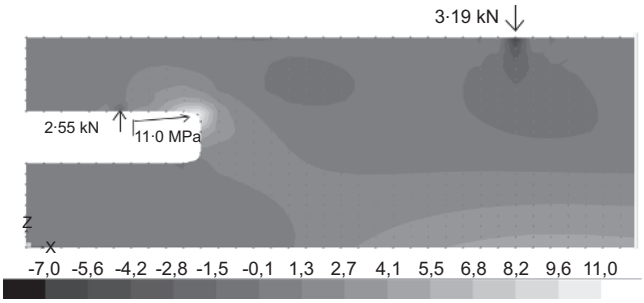

Figure 14. Finite element method calculation of maximum principal stresses at bottom of kerf: Lioz limestone

(K_t) and the stress concentration caused by the intrinsic brittle behaviour of each type of stone (M_c) using the following relationship:

$$9. \quad K_{eff} = K_t \times M_c$$

The magnification factor values, M_c, are thus evaluated for each type of stone (Table 8).

It is interesting to compare the values obtained for M_c with the constant $1 + \tan(\alpha)$ (where α is the average spall angle) [Table 5 – spall angle α measured (Figure 6)] for each stone type (Table 9).

The relationship points to an equation of the following type:

$$10. \quad M_c = 1 + \tan(\alpha)$$

which is like saying that the amplification factor is somehow related with the stone's intrinsic and rheological characteristic. Nevertheless, this relationship is not consistent with any theoretical or other empirical formula. Consequently, emphasis should be placed on the need for further work using other examples of limestone and marble to check whether this relationship is merely coincidental in this case.

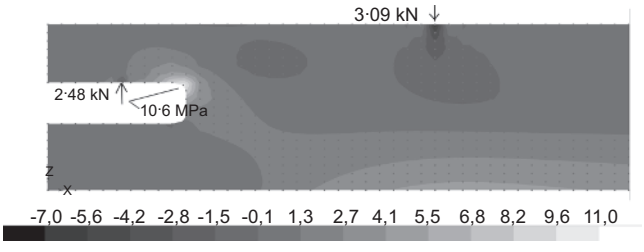

Figure 15. Finite element method calculation of maximum principal stresses at bottom of kerf: Estremoz marble

5.7 Formula for a kerf design anchorage

The ultimate break design load, P_{ud}, must be greater than the wind design acting load:

$$11. \quad P_{Sd} \geq w_{Sd} \times L \times \frac{B}{2}$$

where w_{Sd} is the wind design of dynamic wind pressure; L is the panel span; and B is the panel width.

By combining Equations 5 and 6 with Equation 10 and, for variable C, to solve the clearance or distance between the anchor's contact point and kerf bottom (Figure 10), the following equation is obtained to establish the minimum clearance between the kerf rail and the bottom of the edge groove:

$$12. \quad C \geq \frac{1}{12} \times \frac{(2 \times t_f \times \sigma_{tRd})^2 - (w_{Sd} \times L \times K_{eff})^2}{\sigma_{tRd} \times w_{Sd} \times L \times K_{eff}}$$

Alternatively, it is possible to define the minimum fin thickness by solving Equation 12 for t_f:

$$13. \quad t_f = \frac{\sqrt{12 \times C \times K_{eff} \times w_{Sd} \times L \times \sigma_{tRd} + (w_{Sd} \times L \times K_{eff})^2}}{2 \times \sigma_{tRd}}$$

where C is the clearance between the kerf rail and the bottom of the edge groove; K_{eff} is effective stress concentration factor equal to $K_t \times (1 + \tan\alpha)$; K_t is the elastic geometric stress concentration factor; σ_{tRd} is the design value of the stone's flexural tensile strength equal to MR/γ_M; MR is the flexural strength of the stone; γ_M is a partial safety factor for the tensile strength of the stone; t_f is the fin or leg thickness of the kerfed edge stone; w_{Sd} is the design value of the dynamic wind pressure; L is length or span of the supported dimension stone; and α is the spall failure angle of the kerfed edge stone.

A comparison was made between the required thickness given by Equation 13, due to the breaking load at the kerf and due to the bending resistance for spans between 500 and 1400 mm.

The total required thickness at the edge is calculated assuming that the groove has a typical width of 7 mm, a clearance of $C = 15$ mm, a flexural strength of $FS = 20$ MPa, $\gamma_M = 4$, $K_{eff} = 2$ and for a wind design value of $w_{Sd} = 2{\cdot}0$ kPa.

Partial safety factors were used in this example. However, it is reasonable to assume that an allowable stress approach, with a global safety factor, would yield similar results.

(1)	(2)	(3)	(4)	(5)	(6)
Stone	Type	*P*: kN Figure 7	σ_{max} FEM: MPa	σ_{max} Equation 8: MPa	σ_{nom} Equation 5: MPa
Molianos	Limestone	1·65	7·0	6·8	4·29
Lioz	Limestone	2·55	11·0	10·3	6·49
Estremoz	Marble	2·48	10·6	10·0	6·32

Table 6. Peak stresses obtained using Equation 8 and finite element method (FEM) for each stone type

Stone	Type	σ_{max} FEM: MPa	σ_{nom} Equation 5: MPa	K_t
Molianos	Limestone	7·0	4·29	1·63
Lioz	Limestone	11·0	6·49	1·69
Estremoz	Marble	10·6	6·32	1·68
	average	–	–	1·67

Table 7. Elastic concentration factors with σ_{max} from finite element method (FEM)

		(1)	(2)	(3)
Stone	Type	K_{eff}	K_t	M_c
Molianos	Limestone	2·12	1·63	1·30
Lioz	Limestone	2·40	1·69	1·42
Estremoz	Marble	3·22	1·68	1·91

Table 8. Stresses from FEM analysis versus peak values using Equation 6 for each stone type

Stone	Type	Spall angle α	$[1+\tan(\alpha)]$	M_c
Molianos	Limestone	15·8°	1·28	1·30
Lioz	Limestone	23·9°	1·44	1·42
Estremoz	Marble	44·5°	1·98	1·91

Table 9. Stress magnification factors compared with the fin's detachment spall angles

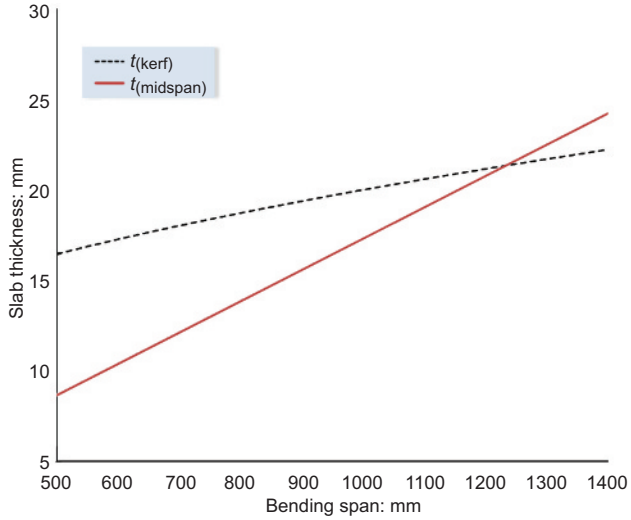

Figure 16. Comparison between calculated thickness for breaking load and bending strength

It seems evident that the required panel thickness is consistently determined by support strength, t_{kerf} rather than by bending at midspan due to flexural resistance (Figure 16).

The authors are of the opinion that stone panel thickness design will be unsafe if it continues to emphasise bending strength over anchorage breaking load, as is common practice.

5.8 Safety factors design

Allowable stress design factors were applied based on the stone's physical/mechanical properties determined by testing that particular stone. In this field, some further work and tests are still necessary in order to establish adequate partial safety factors based on reliability calibration. Until that time, global safety factors based on allowable stresses may be used.

For example, based on recommendations by the Marble Institute of America (2008) a global safety factor of 3 is usually used for granite panel stresses away from connections, and a safety factor of 4 is usually used for stresses in the granite at connections. Based on the said Institute's recommendations, a safety factor of 5 is commonly used for marble panel stresses caused by wind loading. For travertine, limestone and quartz-based stone, a safety factor of 8 is recommended. The Indiana Limestone Institute Handbook (1989) recommends that a safety factor of 6 be used for Indiana Limestone.

6. Conclusion

It has been shown that a design focused on the bending strength of stone panels, to the detriment of the kerf anchorage, is unsafe. Yet, normal practice, as mentioned above, does not take this into account.

In designing stone cladding systems with continuous kerf, two different effects must be taken into account when evaluating

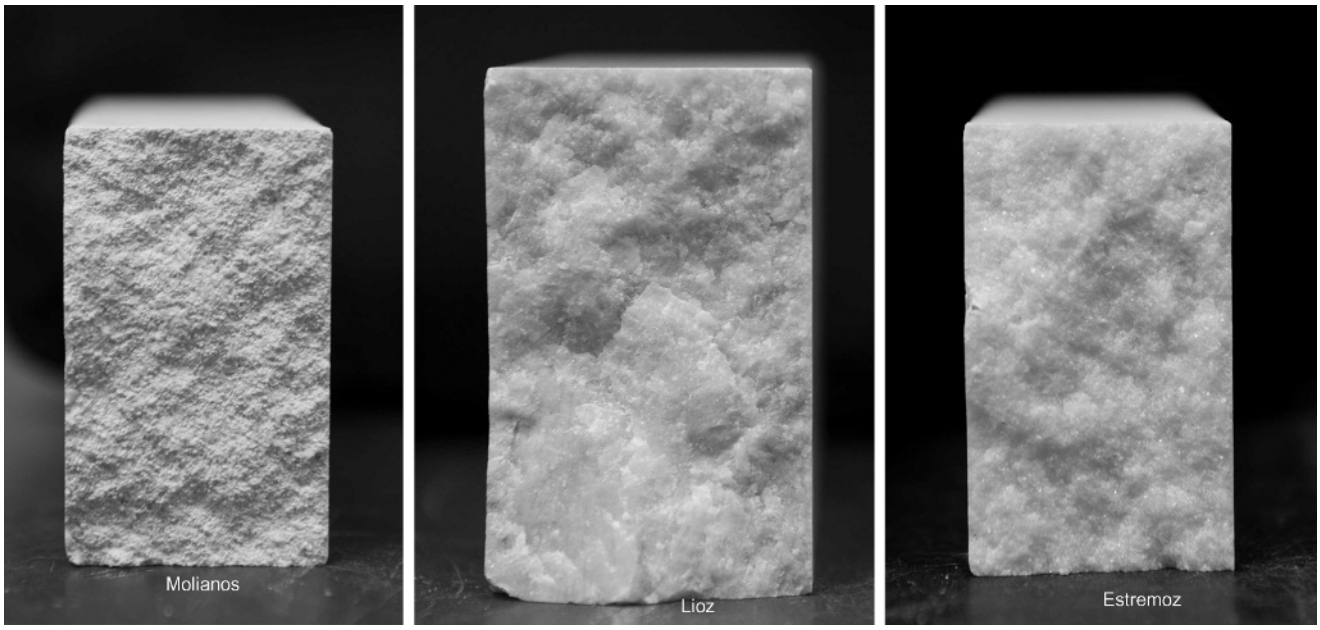

Figure 17. From left to right, different metamorphism stages: lower degree of crystallization in Molianos and Lioz limestone and a higher level of metamorphism in the Estremoz marble

the effective stress in the critical region (kerf's leg): first, the kerf geometry and, second, the stone-specific properties.

The first factor (kerf geometry) will cause stress concentration near the critical region that can be determined through analytical or numerical methods. The second factor (stone properties) further amplifies the stress, typical of quasi-brittle stones, and can be determined only through laboratory testing.

The computed magnification factor values (column 3 of Table 8) are directly related to the type of stone studied in addition to its rheological properties, mineralogical flaws and grain structure.

The stress magnification factor depends on the observed spall angle, and it seems evident that this angle is somehow related to the type of stone.

It can be observed – such as in the case of Molianos, an oolitic limestone which is practically non-crystalline and with a regular internal structure (Figure 17, left) – that the spall angle is low and, consequently, the magnification factor is also low.

For the Lioz**,** a semi-crystalline limestone with coarse elements and slightly affected by metamorphism (Figure 17, centre), the spall angle increases slightly when compared with the previous stone and, consequently, the magnification factor also increases accordingly.

Lastly, the Estremoz marble has a higher level of metamorphism leading to a higher degree of recrystallisation (Figure 17, right), and thus it was found to have a greater spall angle and magnification factor.

The derived semi-empirical formulae make it possible to evaluate the thickness required for a particular type of stone with kerfed edges in a continuous stiff rail.

It must be emphasised that the stress concentration factor is not a safety factor. Regardless of the applied design principles, the safety factors must be applied after computing the effective stresses, taking into account relevant situations of geometry and the degree of metamorphism for each type of stone.

REFERENCES

Albrecht P and Yamada K (1977) Rapid calculation of stress intensity factors. *Journal of the Structural Division, ASCE* **103(2)**: 377–389.

ASTM (2003) ASTM C 1242 – 03: Standard guide for selection, design, and installation of exterior dimension stone anchors and anchoring systems. ASTM, West Conshohocken, PA, USA.

ASTM (2004) ASTM C 1354 – 96: Standard test method for strength of individual stone anchorages in dimension stone. ASTM, West Conshohocken, PA, USA (Reapproved 2004).

Camposinhos RS and Amaral P (2007) *Technical Manual on the Application, Use and Maintenance of Ornamental Stone.* Assimagra – Associação Portuguesa dos Industriais de Mármore, Granitos e Ramos Afins, Lisbon, Portugal, p. 45.

Camposinhos SR and Camposinhos RPA (2009) Dimension stone cladding design with dowel anchorage. *Proceedings of the Institution of Civil Engineers – Construction Materials* **162(3)**: 95–10.

CEN (European Committee for Standardization) (1999) EN 12372 – Determination of flexural strength under concentrated load. CEN, Brussels, Belgium.

CEN (2006) EN 1926 – Determination of uniaxial compressive strength. CEN, Brussels, Belgium.

Conroy K and Hoigard KR (2007) Stiffness considerations in dimension stone anchorage. *Dimension Stone Use in Building Construction* (Kurt R. Hoigard and Michael J. Scheffler (eds)). ASTM, West Conshohocken, PA, USA.

Indiana Limestone Institute of America (1989) *Indiana Limestone Institute of America, Inc. Handbook,* 22nd edn. Indiana Limestone Institute of America, Bedford, IN, USA.

Lammert BT and Hoigard KR (2007) Material strength considerations in dimension stone anchorage design. *Dimension Stone Use in Building Construction* (Kurt R. Hoigard and Michael J. Scheffler (eds)). ASTM, West Conshohocken, PA, USA.

Lewis MD (1995) *Modern Stone Cladding: Design and Installation of Exterior Dimension Stone Systems*. ASTM, West Conshohoken, PA, USA.

Lewis MD (2007) Status on development of code requirements for exterior stone cladding. *Dimension Stone Use in Building Construction* (Kurt R. Hoigard and Michael J. Scheffler (eds)). ASTM, West Conshohocken, PA, USA.

Marble Institute of America (2008) *Dimension Stone Design Manual, VII*. Marble Institute of America, Cleveland, OH, USA.

Moreiras STF, Paraguassu AB and Ribeiro RP (2007) Dimension stone for building façades: methodology for structural design. *Bulletin of Engineering Geology and the Environment* **67(1)**: 53–57.

Pilkey W and Pilkey D (2007) *Petersin's Stress Concentration Factors*. John Wiley, NJ, USA.

Rooke DJ and Cartwright DP (1976) *Compendium of Stress Intensity Factors*. HMSO, London, UK.

Sauoma V, Natekar D and Hansen E (2003) Cohesive stresses and size effects in elasto-plastic and quasi-brittle materials. *International Journal of Fracture*, 2003, **119(3)**: 287–298.

Shah SP, Swartz SE and Ouyang C (1995) *Fracture Mechanics of*

Concrete: Applications of Fracture Mechanics to Concrete, Rock, and Other Quasi-brittle Materials. John Wiley, New York, NY, USA.

West D (2004) Safety factors for design of thin granite cladding – a review of international practice. *Discovering Stone* **3(5)**: 44–46.

West DG and Heinlin M (2000) Anchorage pullout strength in granite: design and fabrication influences. In *ASTM STP 1394. Dimension Stone Cladding: Design, Constructionm, Evaluation, and Repair* (Hoigard KR (ed.)). ASTM, West Conshohocken, PA, pp. 121–134.

WHAT DO YOU THINK?

To discuss this paper, please email up to 500 words to the editor at journals@ice.org.uk. Your contribution will be forwarded to the author(s) for a reply and, if considered appropriate by the editorial panel, will be published as discussion in a future issue of the journal.

Proceedings journals rely entirely on contributions sent in by civil engineering professionals, academics and students. Papers should be 2000–5000 words long (briefing papers should be 1000–2000 words long), with adequate illustrations and references. You can submit your paper online via www.icevirtuallibrary.com/content/journals, where you will also find detailed author guidelines.